

Figure 1. Definition of geophysical parameters: θ , the incidence angle, and χ , the azimuth angle.

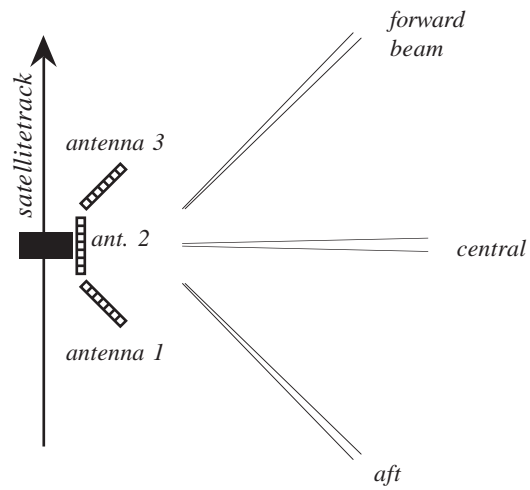


Figure 2. Arrangement of the three antennas for the ERS-1/2 scatterometers.

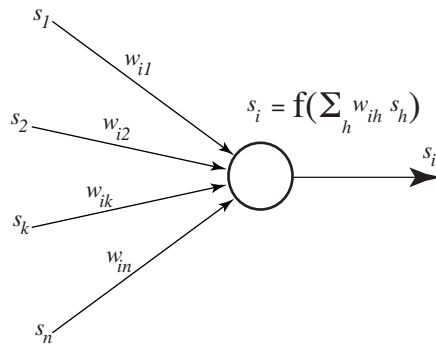


Figure 3. Representation of a neuron.

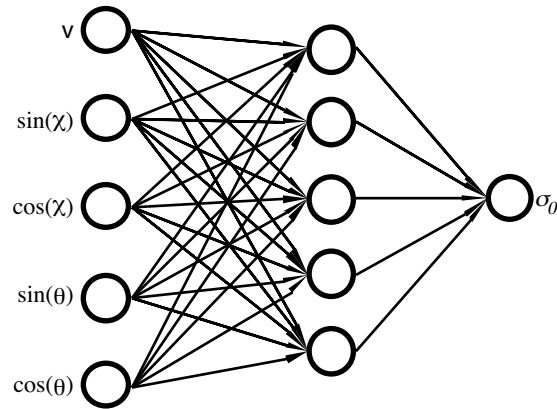


Figure 4. Architecture of the four NN-GMF.

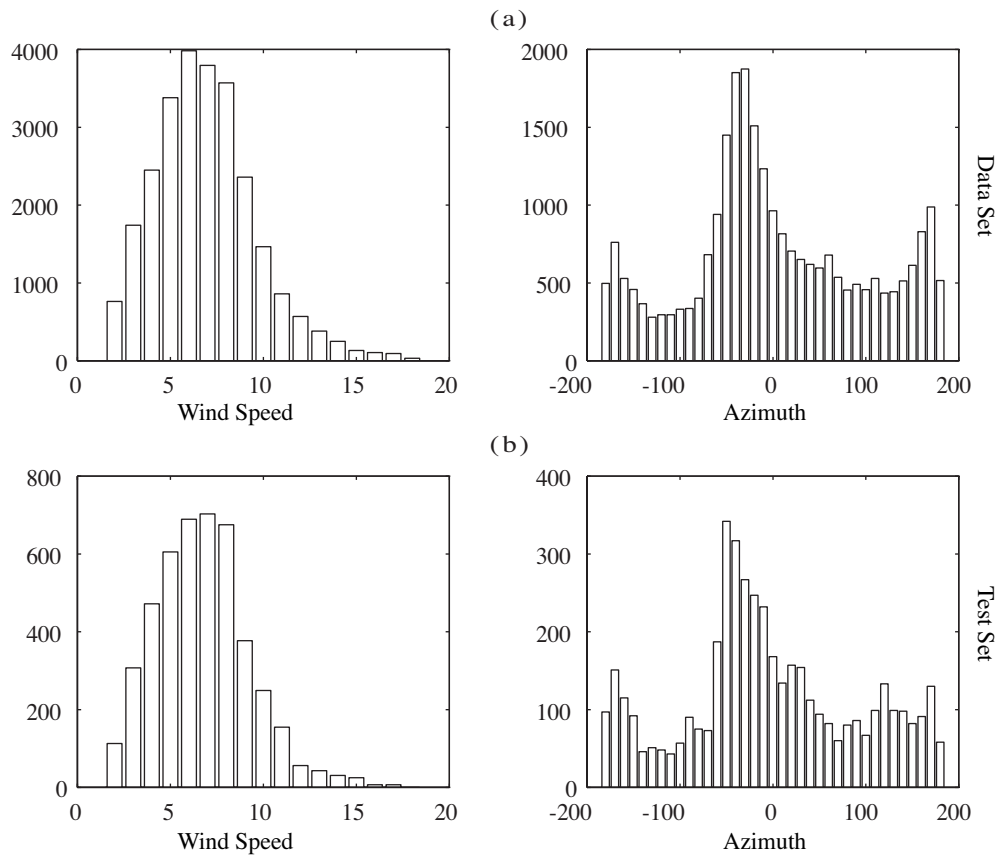


Figure 5. Distribution of wind speed and of azimuth angle in the overall data set (a) and test set (b)

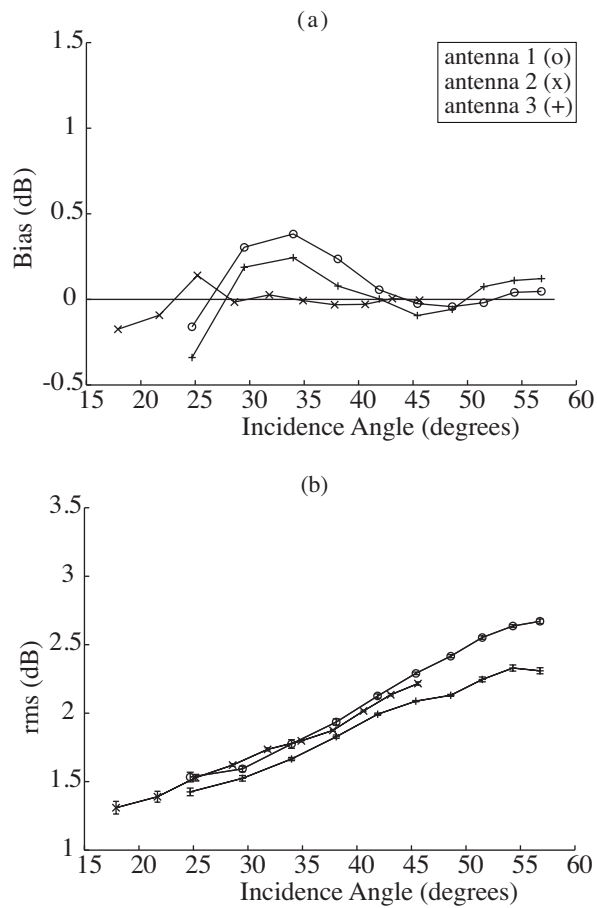


Figure 6. Bias (a) and RMS (b) for NN-A1, NN-A2 and NN-A3 GMFs with respect to the incidence angle.

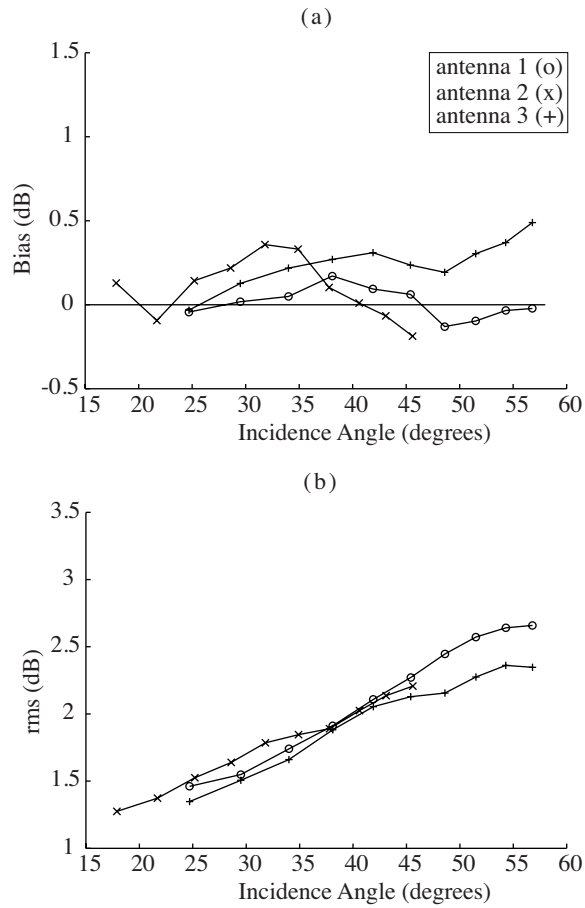


Figure 7. Bias (a) and RMS (b) computed for each antenna with respect to the incidence angle by using the NN-C GMF.

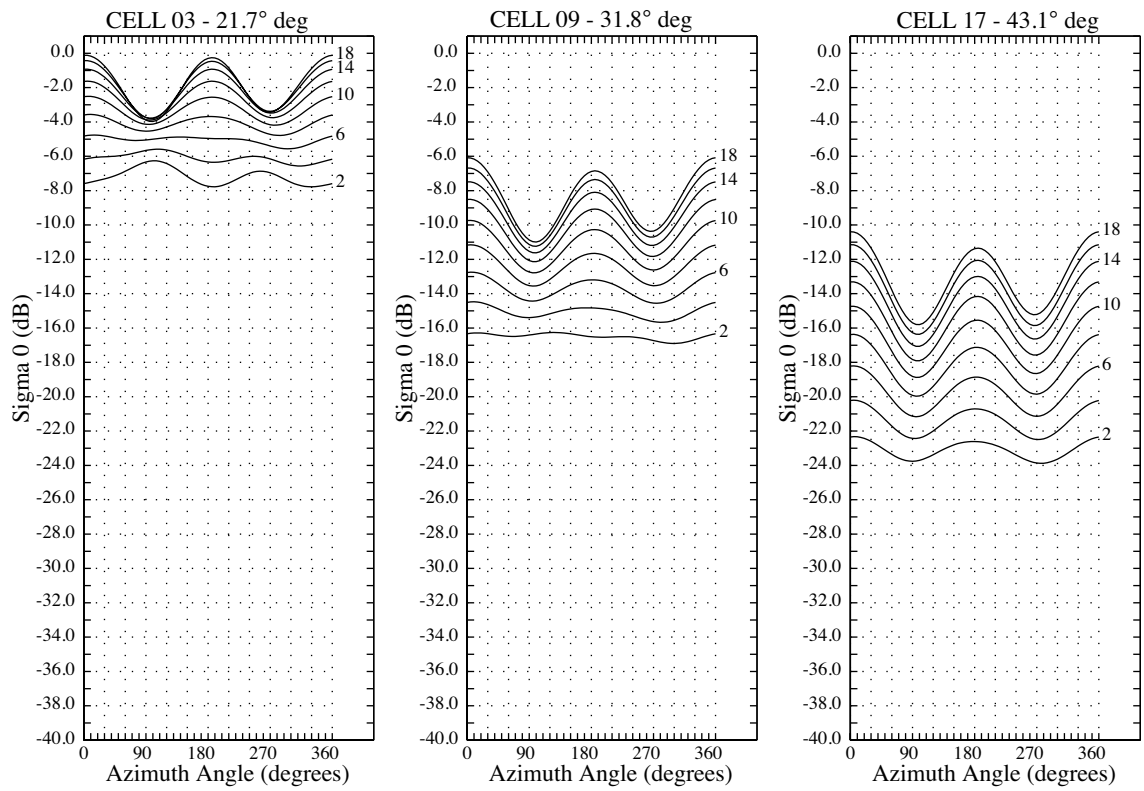


Figure 8. Sigma-0 (in db.) of the NN-C GMF function with respect to the azimuth angle at different wind speeds for different incidence angles. (a) $\theta=21^\circ$; (b) $\theta=31^\circ$; (c) $\theta=43^\circ$.

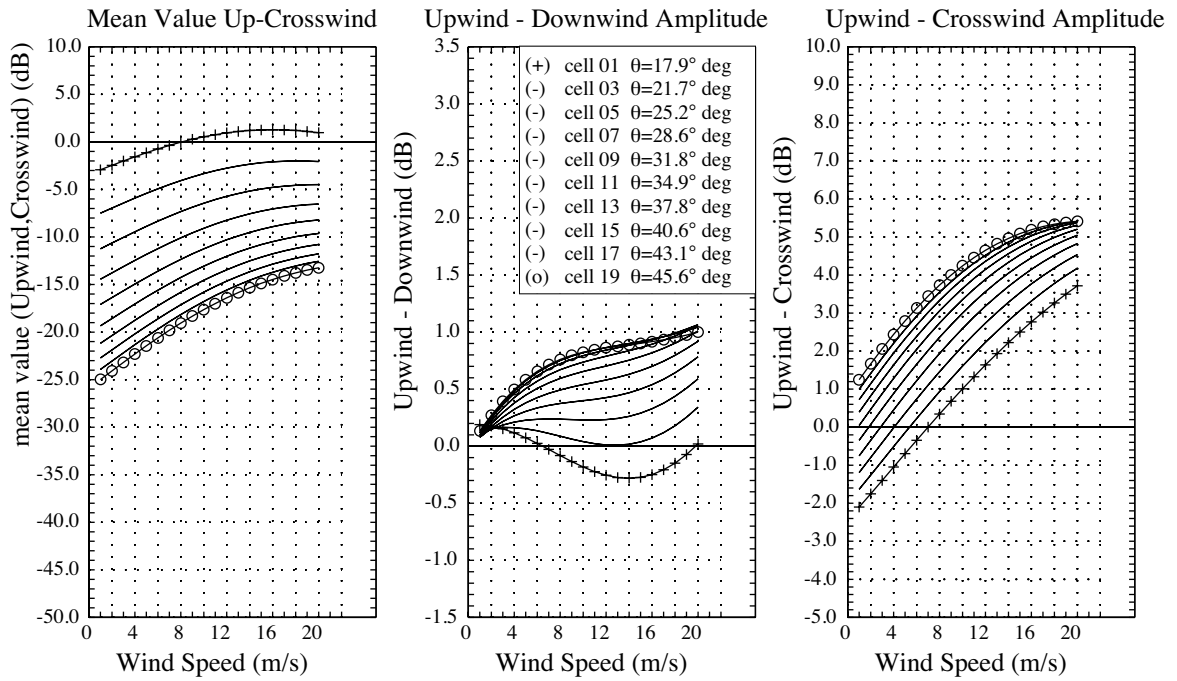


Figure 9. Mean value (a), up-wind minus down-wind (b) and up-wind minus cross wind values (c) with respect to the wind speed at different incidence angles of the NN-C GMF. All these values are given in db.

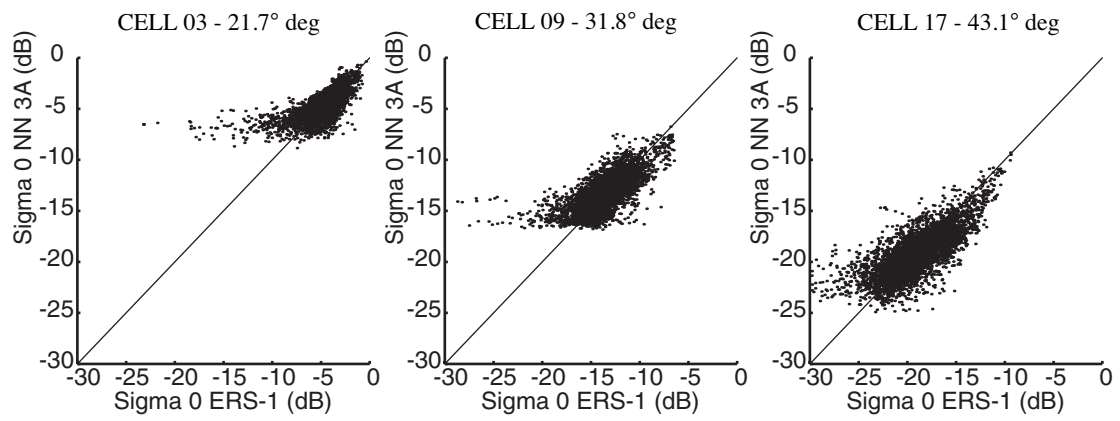


Figure 10. Scatter plots of the NN-C GMF function for the central antenna (A2) at different incidence angles. (a) 21°7; (b) 31°8; (c) 43°1

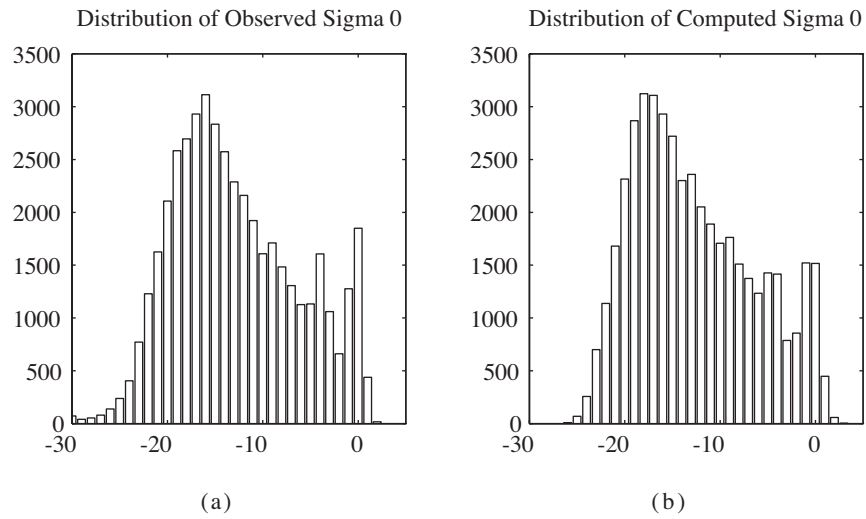


Figure 11. Comparison between the distribution of the observed sigma-0 (a) and this computed by the NN-C GMF function (b) The distributions use all the available sigma-0

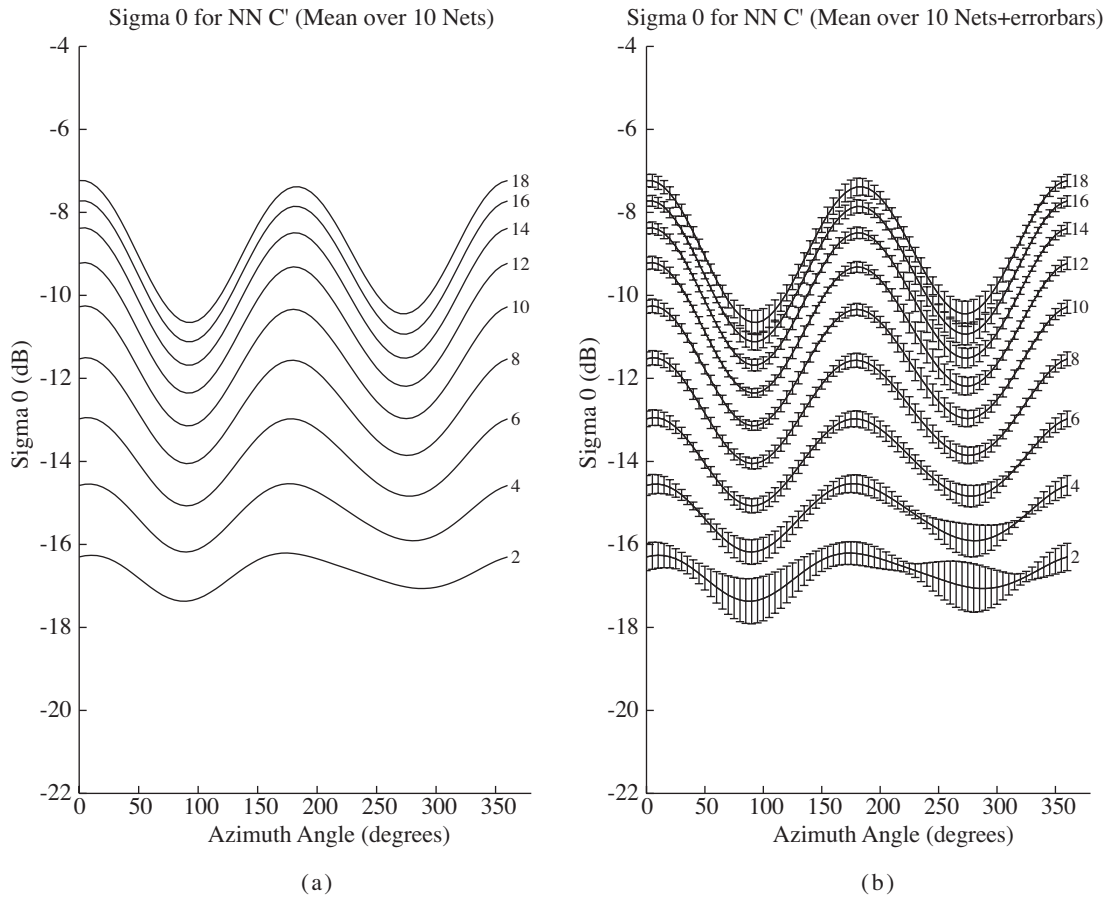


Figure 12. (a) Sigma-0 of the NN-C' GMF function with respect to the azimuth angle at different wind speeds at an incidence angle of $31^{\circ}8$. NN-C' GMF was obtained by averaging 10 different estimated NN-C GMF; (b) The estimated error bars for NN-C'.

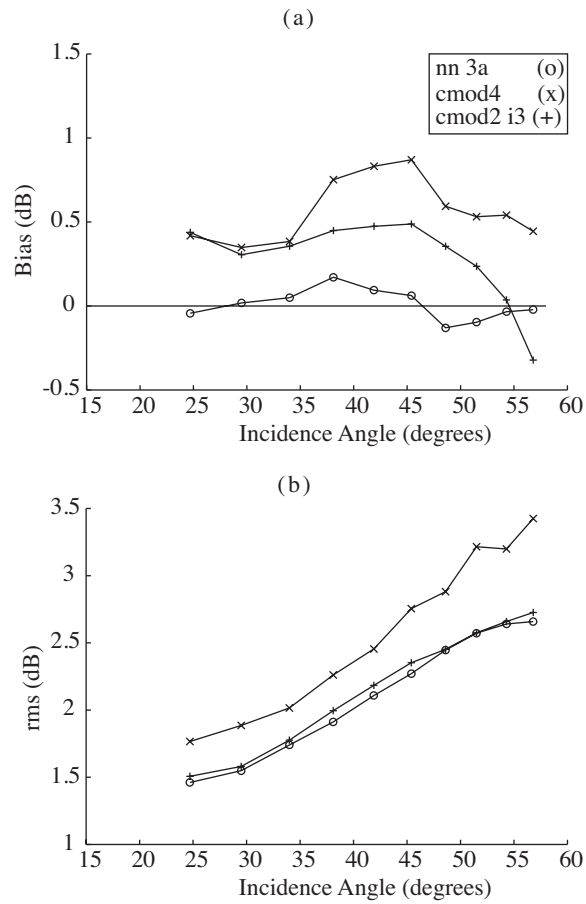


Figure 13. Comparison of the Bias (a) and the RMS (b) of antenna 1 computed with NN-C, CMOD4 and CMOD2-I3 with respect to the incidence angles

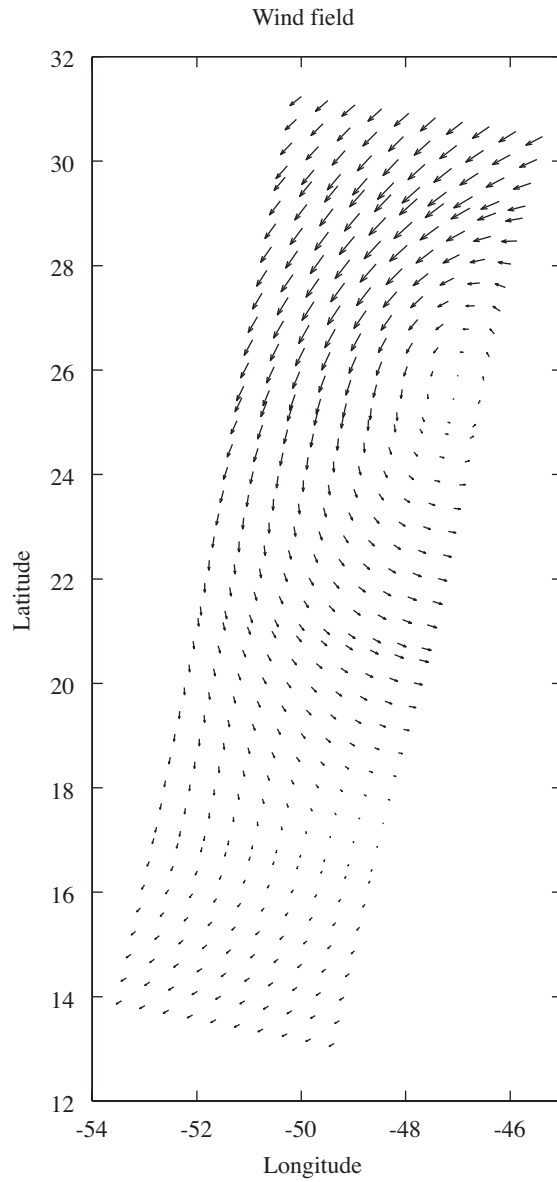


Figure 14. The selected wind field from ECMWF model (Fev-93).

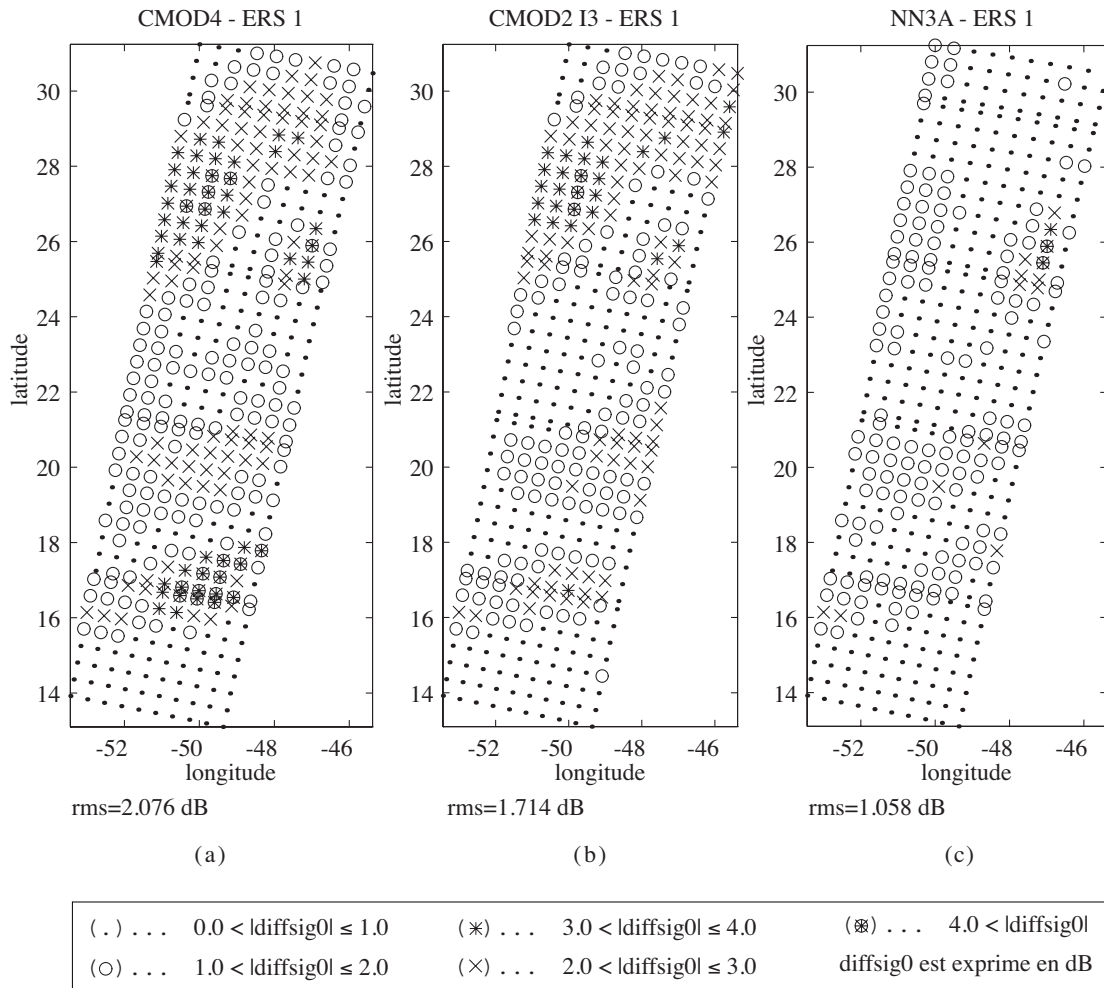


Figure 15. Absolute difference (denoted diffsig0 - in dB) between the observed σ_0 and the computed σ_0 for (a) CMOD4, (b) CMOD2-I3 and (c) NN-C for the meteorological situation presented in figure 14. The computed mean RMS shows that NN-C presents the best skill.

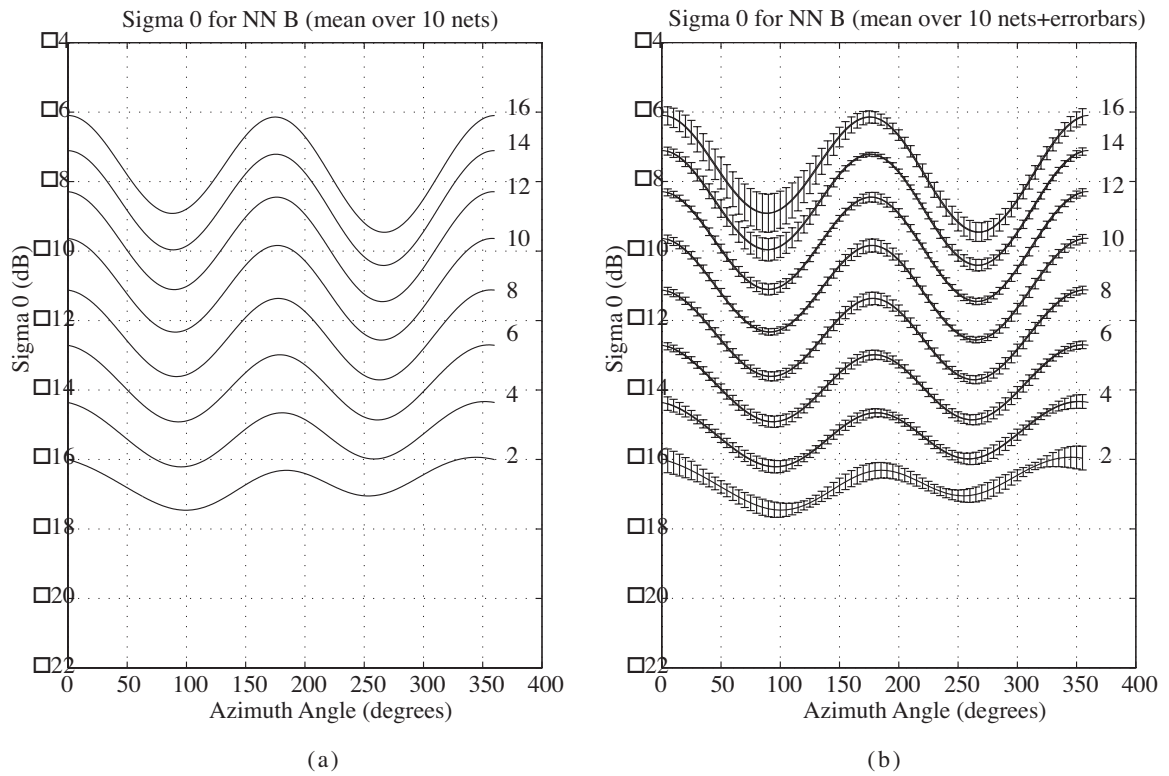


Figure 16. (a) Sigma-0 of the NN-B GMF function with respect to the azimuth angle at different wind speeds at an incidence angle of 31° . (b) the error bars of the NN-B GMF

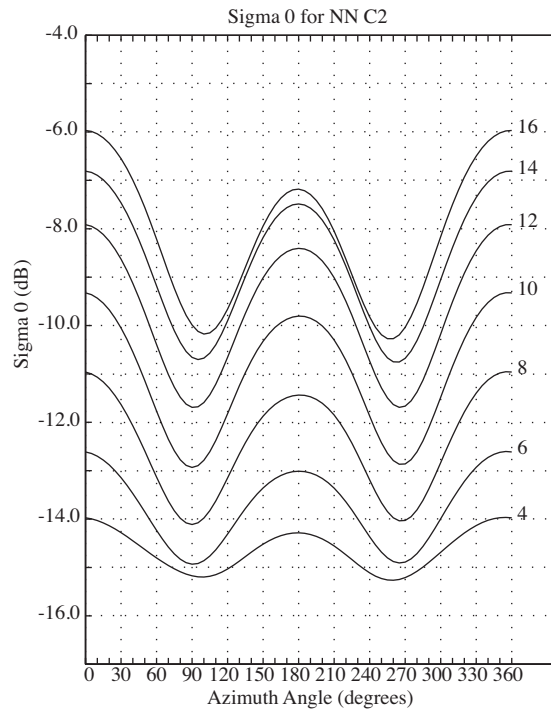


Figure 17. Sigma-0 of the NN-C2 GMF function with respect to the azimuth angle at different wind speeds at an incidence angle of 31°8.